Int. J. Electrochem. Sci., 14 **(2019)** 3968 – 3977, doi: 10.20964/2019.04.65

International Journal of
ELECTROCHEMICAL
SCIENCE
www.electrochemsci.org

Pulse Potentiostatic Deposition of Polyaniline Nanobumps on 3D Graphene Hydrogel for High-Performance Supercapacitor Electrode

Yadong Wang[1], Hanfang Feng[1], Pei Dong[1], Jun Shi[1], Guixun Li[2,], Li Zhang[1,*]*

[1] School of Materials Science and Engineering, Zhengzhou University, Zhengzhou 450001, P. R. China
[2] Department of Civil Engineering Mechanics, Yellow River Institute of Hydraulic Research, Zhengzhou 450003, P. R. China
[*]E-mail: lizhang9@zzu.edu.cn (L. Zhang); liguixun@qq.com (G. Li)

Received: 6 January 2019 / *Accepted:* 22 February 2019 / *Published:* 10 March 2019

The facile pulse potentiostatic method (PPM) was employed to deposit polyaniline (PANI) nanobumps on the framework of hydrothermal graphene hydrogel (GH) in this work. The obtained GH/PANI composite shows larger accessible surface area and higher electrochemical activity than the previous one by the potentiostatic method, thus resulting in the further improvement of electrochemical capacitive properties. The PPM GH/PANI composite exhibits a high specific capacitance (864 F g^{-1} at 2 A g^{-1}), good rate capability (66% capacitance retention even at 100 A g^{-1}), and excellent stability (83% retention after 1000 cycles at 4 A g^{-1}). These results suggest a great advantage of PPM GH/PANI composite electrode for the high performance supercapacitor.

Keywords: Graphene hydrogel; Polyaniline nanobumps; Pulse potentiostatic method; Supercapacitor

1. INTRODUCTION

Supercapacitors (SC), as a promising candidate for energy storage devices, have aroused intense interest owing to their exotic properties of high power density, long cycle life and fast charge/discharge rates[1,2]. However, the relatively low energy density compared with lithium ion batteries or fuel cells still restrains their wide range of practical application[3]. It has been proved that the energy density of SC can be dramatically improved by developing the hybrid electrode materials with advanced microstructure for fully exploiting the merits of electrical double layer (EDL) capacitance and pseudocapacitance. Recently, particular attention has been paid on constructing 3D graphene/ polyaniline (PANI) composite electrodes[4-7], which were found to bring forth a great increase in specific capacitances as well as energy densities, mainly due to their optimized porous structures and

synergetic advantages of 3D graphene (EDL capacitance) and PANI (pseudocapacitance). In our previous work[8], PANI thin layer was also deposited on the 3D framework of graphene hydrogel (GH) via potentiostatic method (PM), and the formed GH/PANI composite electrode has undamped macroporous structure and large surface area, thus showing the significantly improved capacitive behavior (710 F g^{-1} at 2 A g^{-1}) and a good rate capability (73% retention at 100 A g^{-1}). Based on these results, herein, we utilize the pulse potentiostatic method (PPM) to rapidly grow PANI nanobump on the GH skeleton, which leads to the even higher active surface area and fully utilization of PANI pseudocapacitance, accordingly resulting in the further improvement of electrochemical capacitive properties.

2. EXPERIMENTAL

2.1 Materials

Graphite powder (325 mesh) was obtained from Qingdao Huatai Lubricant Sealing S&T Co. Ltd. (Qingdao, China). Aniline (Tianjin Damao Chemical Reagent Factory) was distilled under reduced pressure before use. All other chemicals were of analytical grade and directly used as received.

2.2 Synthetic procedures

Graphene oxide (GO) was prepared using a modified Hummers' method[9]. The GH was prepared through a simple hydrothermal method[10]. A 10 mL portion of GO aqueous dispersion (2 mg mL^{-1}) was transferred to a 16 mL Teflon-lined autoclave and heated at 180℃ for 12 h. After the autoclave was cooled to room temperature, the as-prepared GH was cut into small slices (thickness about 1mm) and stored in deionized water for later use.

Preparation of GH/PANI composites were carried by the PPM using a CHI 660E electrochemical workstation in a three-electrode cell. A slice of GH was tied on a Pt plate with gauze and used as a working electrode, the counter electrode and the reference electrode were the other Pt foil and saturated Ag/AgCl, respectively. The electrolyte is a mixed solution of 1 M H_2SO_4 and 0.5 M aniline. For the pulse potentiostatic deposition, the upper and lower potential were 0.9 and 0 V, respectively. The time durations at both upper potential and lower potential in one pulse were all 1 s. The samples obtained with different pulse cycle numbers of 100, 300 and 500 were denoted as GP100, GP300 and GP500, respectively. The resulting composites were rinsed repeatedly with deionized water to remove unreacted aniline monomer.

2.3 Characterizations

Fourier transform infrared (FTIR) spectrum were recorded on a Spectrum GX FTIR system (PerkinElmer). Raman tests were performed on a RM 2000 Microscopic confocal Raman spectrometer (Renishaw PLC, England) with a 514 nm wavelength laser. The Scanning electron micrographs (SEM) images of the samples were taken by a Hitachi S-5500 field-emission scanning electron microanalyzer.

Nitrogen sorption isotherm and micropore analysis were determined on a TriStar II 3020 instrument at liquid nitrogen temperature. Elemental analysis was collected on a Vario EL/micro cube (elementar, Germany) elemental analyzer.

2.4 Electrochemical measurements

Electrochemical tests were measured on a electrochemical workstation (CHI 660E,CH instrument inc.) with a three-electrode cell. The GH or GH/PANI composite was immersed in electrolyte of 1 M H_2SO_4 solution as the working electrode. The counter and reference electrode were a Pt plate and saturated Ag/AgCl, respectively. The applied potential windows of cyclic voltammetry (CV) and galvanostatic charge/discharge (GCD) measurements all were 0-0.8 V. Electrochemical impedance spectroscopy (EIS) tests in the frequency range of 10^5-0.01 Hz with a amplitude of 10 mV. The mass specific capacitances (C_s) were calculated by GCD measurements using the equations $C_s = I\Delta t/(m\Delta V)$, where I is the constant discharge current, Δt is the discharging time, m is the mass of single electrode, ΔV is the voltage drop upon discharging (excluding the IR drop).

3. RESULTS AND DISCUSSION

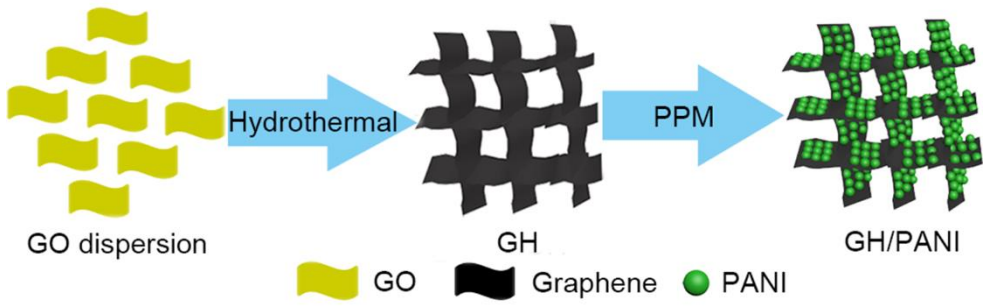

Figure 1. Schematic illustration for the synthetic process of GH/PANI

Compared with the conventional potentiostatic and potentiodynamic method, the pulse potentiostatic deposition for PANI is more facile and simply controlled, and can rapidly grow high-quality polymer with desired nanostructures[11,12]. Here, PPM was employed to deposit PANI on the framework of hydrothermal graphene hydrogel, and the fabrication process is illustrated in Fig. 1. The morphologies of obtained GH/PANI composites with different deposition time were observed by SEM. From Fig. 2a and b, the bare GH presents an interconnected porous structure with micrometer-scale pore size. After PANI was deposited for 100 cycles, GP100 shows a quite similar morphology to the native structure of GH except for the slightly thicker sheets (Fig. 2c and d), which could be ascribed to the low loading amount of PANI. When the deposition cycles is up to 300, the PANI nanobumps are found to uniformly grow on the surface of graphene sheets (GP300 in Fig. 2e and f). With the deposition process further going on, the PANI nanobumps began to branch and form the nanofibers with a diameter of 100

nm and length of 0.1-1 μm (GP500 in Fig. 2g and h). Besides, the deposition amount of PANI can be easily controlled by deposition cycles. The weight fractions of PANI in composites with different pulse cycles were measured by element analysis, as shown in Table 1. Noticeably, the weight content of PANI (36%) in GP300 is obtained only for about 10 min by the PPM, which is higher than that of GP20 (29%) by PM for 20 min, indicating the faster growth of the PANI by PPM.

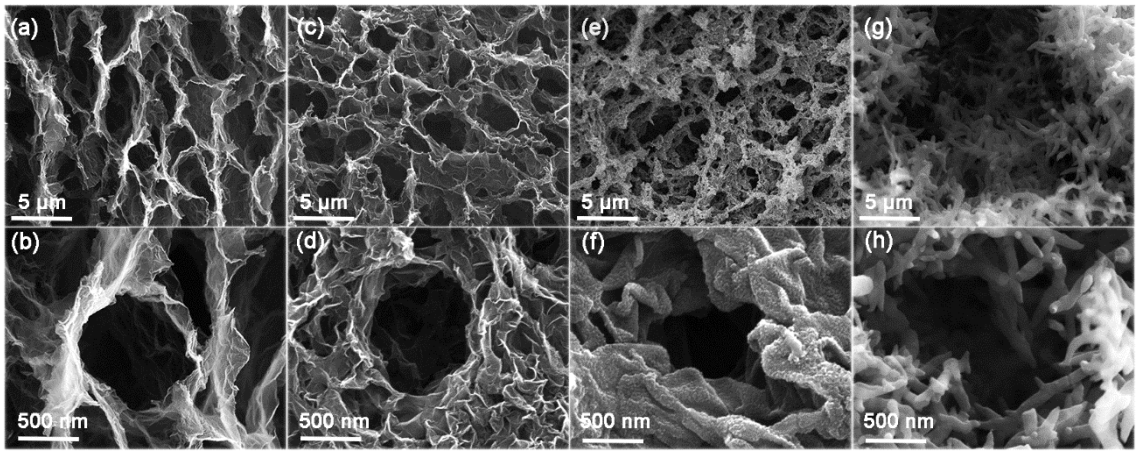

Figure 2. SEM images with different magnification of GH (a, b), GP100 (c, d), GP300 (e, f) and GP500 (g, h)

It is obvious that the whole growth process of PANI on GH prepared by PPM is totally different from the previous one by PM[8]. Several possible reasons can be considered to explain these differences. (i) PPM provides the incontinuous and dynamic deposition process of PANI. At the very beginning of deposition, the PANI chain nucleates on the graphene surface in a short pulse-on period, forming the partially covered nucleation region[12]. In the subsequent pulses, the fresh PANI nucleation was frustrated due to the transient deposition time, and hence the consecutive growth of PANI chains over the pre-existing nucleation sites on graphene surface become likely[13]. This fast nuclei formation favours homogeneous nucleation and decreases the opportunity of heterogeneous nucleation [8], which results in the growth of nanobumps and nanofiber structures of PANI. (ii) During pulse cycles, the consumed aniline molecules can be replenished in pulse-off time, and the periodic stretching and relaxing of polymer chains can help aniline molecules access easily[11], thus leading to the fast growth of PANI on GH. (iii) The periodic potential pulse stimulation during PPM allows aniline monomers to deep diffuse into the the internal network of GH, producing a more uniform distribution of PANI and less blocked pores than that obtained with PM. All of these PPM advantages afford the possibility to further promote the electrochemical capacitive properties of GH/PANI composite electrode.

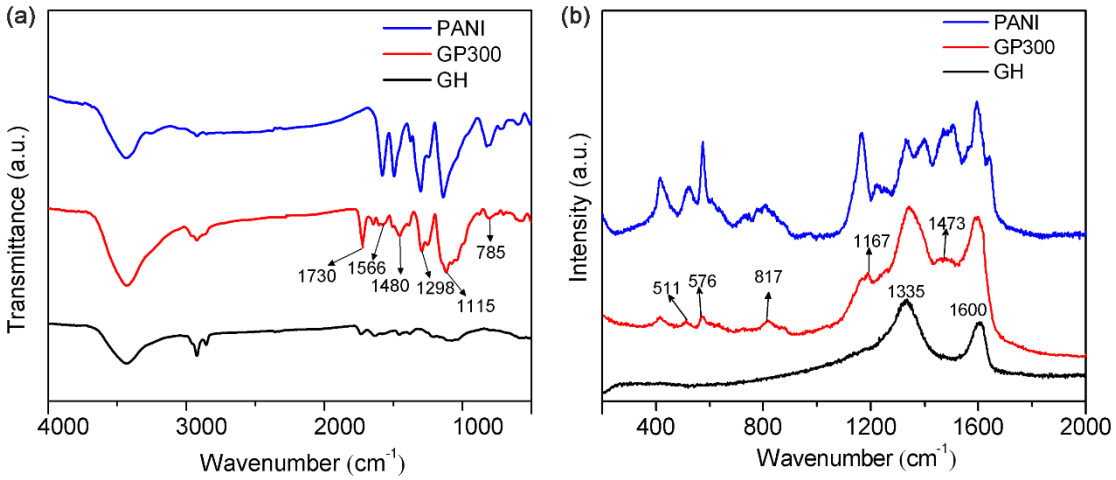

Figure 3. (a) FTIR and (b) Raman spectra of PANI, GP300 and GH

Fig. 3 shows the FTIR and Raman spectra of pure PANI, GP300 and GH. As shown in Fig. 3a, GH presents featured bands attributed to partially reduced GO[15]. After the electrodeposition, the FTIR spectrum of GP300 shows some new bands assigned to PANI, including 1566 cm^{-1} (quinonoid C=C), 1480 cm^{-1} (benzenoid C=C), 1298 cm^{-1} (C-N), 1115 cm^{-1} (C-H in-plane) and 785 cm^{-1} (C-H out-of-plane), suggesting successful deposition of PANI on the framework of GH. Besides, the intensified "electronic-like band" at 1115 cm^{-1} and the red-shift of characteristic peaks compared with pure PANI imply the strong interaction between graphene sheets and PANI[16]. Likewise, from the Raman spectrum of GP300 in Fig. 3b, apart from the D (1335 cm^{-1}) and G (1600 cm^{-1}) bands from GH, some other peaks belonging to doped PANI appear at 511 (phenazine-like), 576 (C-H out-of-plane), 817 (quinonoid C–H), 1167 (benzenoid C–H) and 1473 cm^{-1} (semiquinone radical cation) [7], suggesting successful electrodeposition of PANI on the framework of GH[17].

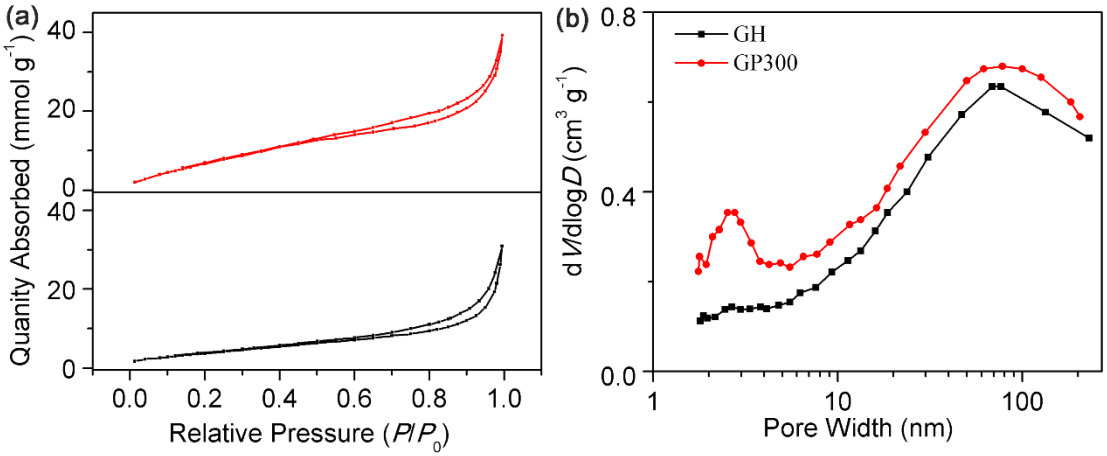

Figure 4. (a) N_2 adsorption-desorption isotherms of GH and GP300 (b) the pore size distribution of GH and GP300

The N_2 adsorption-desorption isotherms and the pore size distribution of GH and GP300 are shown in Fig. 4a and b. Both isotherms are marked by type II isotherm with no hysteresis loops,

suggesting no existence of micropores in these hydrogels. The Brunauer-Emmett-Teller (BET) specific surface area (S_{BET}) value of GP300 is 393 m^2 g^{-1} when it is calculated in terms of the GH and PANI mass, and even as high as 614 m^2 g^{-1} when only considered the GH mass in GP300. The value is almost doubled compared to that of GH (309 m^2 g^{-1}), and is also signally larger than that of PM GH/PANI composite (332 m^2 g^{-1})[8], implying that the PPM deposition for PANI indeed gain a higher surface area of GH/PANI composite. Moreover, GH and GP300 shows similar curve in the range of more than 10 nm, while the evident peaks of the GP300 sample appear in the range of 2-5 nm as a result of the introduction of PANI nanobumps[18], which is also consistent with the SEM results.

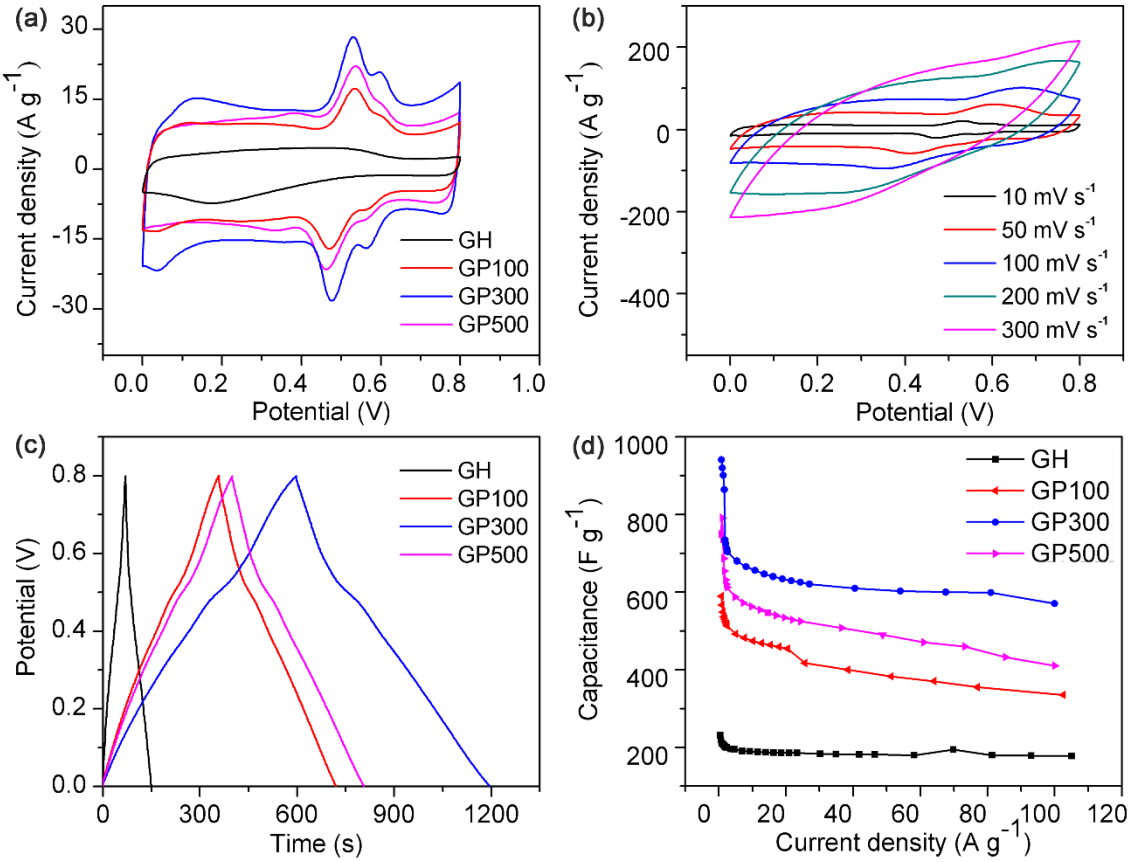

Figure 5. (a) CV curves at 10 mV s^{-1}; (b) CV curves of GP300 at different scan rates; (c) GCD curves at 2 A g^{-1}; (d) Plots of specific capacitance versus current density for GH and GH/PANI composites

The electrochemical capacitive performance of GH/PANI composites prepared by PPM were evaluated by CV and GCD in a three-electrode system. In Fig. 5a, different from the nearly rectangular CV curve for GH, all the GH/PANI composites display enlarged CV curves which reveal the combination of EDL capacitance of GH and faradaic capacitance of PANI[20]. Among them, GP300 possesses the largest CV loop area, indicating the best capacitive performance. Moreover, compared to the GH/PANI composite prepared by PM[8], the more evident redox peaks (0 to 0.2 V) appears in the CV curve of GP300 (Fig. 5a), which can be attributed to the exchange between leucoemeraldine and emeraldine[21], indicating the GH/PANI obtained by PPM shows higher electroactivity than that by PM[8]. Fig. 5b displays the CV behaviors of GP300 at different scan rates. It is obvious that the peak

current densities rise with the increase of scan rates while the CV shapes change little, revealing the fast charge propagation behavior and good rate capability of GP300[22].

Fig. 5c depicts the GCD profiles of the GH and GH/PANI composites. Compared with symmetric triangle curve of GH, all curves of GH/PANI samples show slight curvatures and much longer discharging durations indicative of their pseudocapacitive behavior. The specific capacitances (C_s) are calculated from GCD results and listed in Table 1. The maximum C_s of 864 F g^{-1} is attained with GP300, which is an increase of 22% compared to that of GH/PANI composite prepared by PM (710 F g^{-1})[8]. This improved capacitance is related to the higher electrochemical activity and nanobump structure of PANI deposited on GH by PPM, which further enlarge the accessible surface area and enhance the effective utilization of active materials. By comparison, the lower C_s (551 F g^{-1}) of GP100 might be due to the small amount of deposited PANI in a short periods, and the also slightly lower C_s (647 F g^{-1}) of GP500 can be ascribed to that the full-grown thick PANI nanofiber would decrease the specific surface contribution to the pseudocapacitive charge storage.

Table 1. Specific capacitances (C_s) at different current densities, capacitance retentions (C_r), equivalent series resistance (R_s), and charge transfer resistance (R_{ct}) for various electrode materials

Sample	PANI (wt%)	C_s (F g^{-1}) at 2 A g^{-1}	C_s (F g^{-1}) at 100 A g^{-1}	C_r (%)	R_s (Ω)	R_{ct} (Ω)
GH	0	201	170	85	0.67	1.21
GP100	21	551	329	60	0.78	1.92
GP300	36	864	570	66	0.59	2.22
GP500	52	647	411	64	0.65	2.27

The variations of the C_s values with the current density for all electrodes were plotted in Fig. 5d and the corresponding results are also presented in Table 1. With the current density increasing from 2 to 100 A g^{-1}, GH/PANI composites maintain more than 60% of the initial capacitance. Although these C_s retention are lower than that of GH electrode (85% retention) with fast EDL kinetics, which still among the best in term of rate performance by comparing with other reported GH/PANI composites, as listed in Table 2, implying that depositing PANI nanostructure on 3D GH framework by PPM can provide unobstructed electron and ion transport channel throughout the electrode, thus delivering sufficient capacitance even at fast charging/discharging rates.

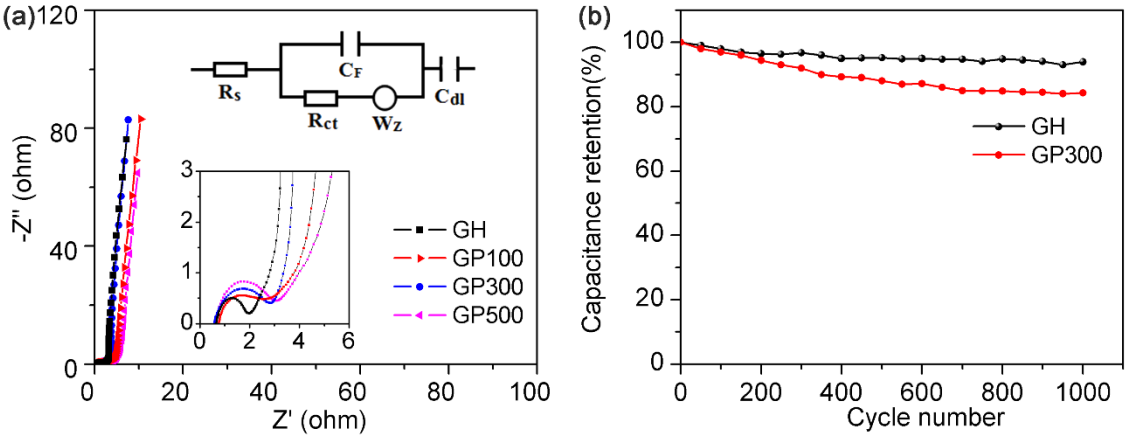

Figure 6. (a) EIS Nyquist plots of GH and GH/PANI composites electrode. (b) Cycling stability of GH and GP300 at 4 A g^{-1}

Table 2. Comparison of electrochemical properties of graphene/PANI composite electrodes

Electrodes	Highest C_s (F g^{-1})	Capacitance retention	References
PANI fibers/CCG	791 (1.1 A g^{-1})	99% (783 F g^{-1}) at 27.3 A g^{-1}	[3]
PANI coating/rGO	193 (1.0 A g^{-1})	89% (171 F g^{-1}) at 50.0 A g^{-1}	[5]
PANI film/3D graphene hydrogel	710 (2.0 A g^{-1})	73% (517 F g^{-1}) at 100.0 A g^{-1}	[8]
PANI nanorods/graphene paper	763 (1.0 A g^{-1})	64% (490 F g^{-1}) at 10.0 A g^{-1}	[17]
PANI arrays/3D rGO	432 (1.0 A g^{-1})	81% (352 F g^{-1}) at 20.0 A g^{-1}	[23]
PANI nanocone arrays/3D graphene network	751 (1.0 A g^{-1})	89% (664 F g^{-1}) at 10.0 A g^{-1}	[24]
PANI nanofibers/N-doped graphene hydrogel	610 (1.0 A g^{-1})	57% (350 F g^{-1}) at 20.0 A g^{-1}	[25]
PANI/rGO pillar	630 (0.5 A g^{-1})	57% (362 F g^{-1}) at 4.0 A g^{-1}	[26]
PANI/rGO hollow sphere	456 (0.5 A g^{-1})	64% (290 F g^{-1}) at 10.0 A g^{-1}	[27]
PANI hollow sphere/rGO	529 (0.5 A g^{-1})	72% (381 F g^{-1}) at 10.0 A g^{-1}	[28]
I-doped PANI/rGO hydrogel	713 (1.0 A g^{-1})	57% (403 F g^{-1}) at 10.0 A g^{-1}	[29]
PANI layer/rGO sheet	875 (1.0 A g^{-1})	65% (569 F g^{-1}) at 10.0 A g^{-1}	[30]
PANI nanofiber/3D graphene foam	968 (0.3 A g^{-1})	27% (263 F g^{-1}) at 12.4 A g^{-1}	[31]
PANI/CCG hydrogel film	450 (5.0 A g^{-1})	96% (432 F/g) at 100.0 A g^{-1}	[32]
PANI nanobumps/3D graphene hydrogel	864 (2.0 A g^{-1})	66% (570 F g^{-1}) at 100.0 A g^{-1}	This work

EIS measurements were carried out to analyze the electrochemical kinetics of GH/PANI composites in the frequency from 10^5 to 0.01 Hz. As shown in Fig. 6a, all EIS Nyquist plots

include the small high-frequency semicircle (charge transfer resistance R_{ct}), middle-frequency Warburg section (impedance W_Z), and low-frequency straight line (capacitance C_F). The X-intercepts at very high frequency indicate the equivalent series resistance of electrode (R_s), which are almost the same for GH and GH/PANI composites (Table 1), revealing deposition of PANI does not affect the electrical conductivity of GH electrode[8]. GH/PANI composites show the larger R_{ct} than GH due to their faradaic reaction process happened on the interface of PANI and electrolyte. Furthermore, GP300 exhibits a short 45° Warburg region and succeeding almost vertical line in the mid-low frequency range, suggesting the fast electrolyte diffusion through the electrode towards ideal capacitive behavior in GP300.

The cycling stability is another important parameter for electrode materials as supercapacitors. Fig. 6b shows the cycling performance of GH and GP300 electrodes using a long-term GCD technique at a 4 A g^{-1}. After 1000 cycles, 90% and 83% of initial capacitances are retained for GH and GP300 electrodes, respectively. The main reason of this excellent stability may be come from that the GH not only provides a flexible and mechanically strong framework, but also strongly adheres PANI through π-π interaction, thus relieving the volume change and mechanical deterioration caused by the swelling and shrinking of PANI[33].

4. CONCLUSION

PPM was employed to deposit PANI nanobumps on the 3D framework of GH to prepare the GH/PANI composite. Due to incontinuous and dynamic trait of PPM, the morphology of PANI evolved from nanobumps to nanofiber with increased deposition cycles. Compared with PM GH/PANI composite, the GP300 exhibits the enhanced capacitive properties with a high C_s (864 F g^{-1} at 2 A g^{-1}), good rate capability (66% retention at 100 A g^{-1}), and excellent stability (83% retention after 1000 cycles at 4 A g^{-1}).

ACKNOWLEDGMENTS
This study was supported by the National Natural Science Foundation of China (No. 21374106), National Key R&D Plan (2018YFD0400702), Fundamental Research Funds for the Central Nonprofit Research Institutions (HKY-JBYW-2017-06) and National Natural Science Foundation of China (No. 51609097).

References

1. J. R. Miller and P. Simon, *Science*, 321 (2008) 651.
2. P. Simon and Y. Gogotsi, *Nat. Mater*., 7 (2008) 845.
3. J. Wu, Q. Zhang, A. Zhou, Z. Huang, H. Bai and L. Li, *Adv. Mater*., 28 (2016) 10221.
4. H. Xu, J. Liu, Y. Chen, C-L. Li, J. Tang and Q. Li, *J. Mater. Sci: Mater. Electron*., 28 (2017) 10674.
5. J. Fernández, J. Bonastre, J. Molina, A.I. del Río and F. Cases, *Eur. Polym. J.,* 92 (2017) 194.
6. X. D. Hong, B. B. Zhang , E. Murphy, J. L. Zou and Kim F, *J. Power Sources*, 343 (2017) 60.

7. L. L. Zhang, D. Huang, N. T. Hu, C. Yang, M Li, H Wei, Z Yang, Y. J. Su and Y. F. Zhang, *J. Power Sources,* 342 (2017) 1.
8. S. Y. Gao, L. Zhang, Y. D. Qiao, P. Dong, J. Shi and S. K. Cao, *Rsc. Adv.,* 6 (2016) 58854.
9. William S. Hummers, Jr. and Richard E. Offeman, *J. Am. Chem. Soc.,* 80 (1958) 1339.
10. L. Zhang and G. Q. Shi, *J. Phys. Chem*. C., 115 (2011) 17206.
11. V. Tsakova, A. Milchev and J. W. Schultze, *Jc Electroanal. Chem.,* 346 (1993) 85.
12. H. F. Jiang and X. X. Liu, *Electrochim. Acta,* 55 (2010) 7175.
13. A. Davies, P. Audette, B. Farrow, F. Hassan, Z. W. Chen, J. Y. Choi and A. P. Yu, *J. Phys. Chem*. C, 115 (2011) 17612.
14. R. K. Sharma, A. C. Rastogi and S. B. Desu, *Electrochem. Commun*., 10 (2008) 268.
15. J. L. Zhang, H. J. Yang, G. X. Shen, P. Cheng, J. Y. Zhang and S. W. Guo, *Chem. Commun*., 46 (2010) 1112.
16. S. Liu, X. H. Liu, Z. P. Li, S. R. Yang and J. Q. Wang, *New J. Chem*., 35 (2011) 369.
17. H. P. Cong, X. C. Ren, P. Wang and S. H. Yu, *Energ. Environ. Sci*., 6 (2013) 1185.
18. C. Yan, Y. W. Kanaththage, R. Short, C. T. Gibson and L. Zou, *Desalination*, 344 (2014) 274.
19. Q. Q. Zhou, Y. R. Li, L. Huang, C. Li, and G. Q. Shi, *J. Mater. Chem*. A, 2 (2014) 17489.
20. Y. F. Wang, X. W. Yang, L. Qiu, and D. Li, *Energ. Environ. Sci*., 6 (2013) 477.
21. X. X. Liu, L. J. Bian, L. Zhang and L. J. Zhang, *J. Solid State Electrochem*., 11 (2007) 1279.
22. R. Liu, J. Duay and S. B. Lee, *Chem. Commun*., 47 (2011) 1384.
23. Y. Yang, Y. L. Xi, J. Z. Li, G. D. Wei, N. I. Klyui and W. Han, *Nanoscale Res. Lett.,* 12 (2017) 394.
24. M. Yu, Y. Ma , J. Liu and S. Li, *Carbon*, 87 (2015) 98.
25. J. W. Luo, W. B. Zhong, Y. B. Zou, C. L. Xiong and W. T. Yang, *J. Power Sources*, 319 (2016) 73.
26. P. Kumari, K. Khawas, S. Nandy and B. K. Kuila, *Electrochim. Acta*, 190 (2016) 596.
27. J. Luo, Q. Ma, H. H. Gu, Y. Zheng and X. Y. Liu, *Electrochim. Acta*, 173 (2015) 184.
28. W. Q. Dai, L. Ma, M. Y. Gan, S. Y. Wang, X. W. Sun, H. H. Wang, H. N. Wang and T. Zhou, *Mater. Res. Bull.,* 76 (2016) 344.
29. J. Wang , B. Li, T. Ni, T. Dai and Y. Lu, *Compos. Sci. Technol*., 109 (2015) 12.
30. P. Sekar, B. Anothumakkool and S. Kurungot, *Acs Appl. Mater. Interfaces*, 7 (2015) 7661.
31. J. Pedros, A. Bosca, J. Martinez, S. Ruiz-Gomez, L. Perez, V. Barranco and F. Calle, *J. Power Sources,* 317 (2016) 35.
32. Y. F. Wang, X. W. Yang, A. G. Pandolfo, J. Ding and D. Li, *Adv. Energy Mater*., 6 (2016) 1600185.
33. D. Jain, S. A. Hashmi and A. Kaur, *Electrochim. Acta*, 222 (2016) 570.